

## Atomistic mechanism of cadmium incorporation into hydroxyapatite

HUAN LIU<sup>1</sup>, XIANCAI LU<sup>1,\*</sup>, XIANGJIE CUI<sup>1</sup>, LIJUAN ZHANG<sup>2</sup>, AND TING-SHAN CHAN<sup>3</sup>

<sup>1</sup>Key Laboratory of Surficial Geochemistry, Ministry of Education, School of Earth Sciences and Engineering, Nanjing University, Nanjing, Jiangsu 210023, China

<sup>2</sup>Shanghai Synchrotron Radiation Facility, Shanghai Advanced Research Institute, Chinese Academy of Sciences, Shanghai 201204, China

<sup>3</sup>National Synchrotron Radiation Research Center, Hsinchu 30076, Taiwan

### ABSTRACT

Hydroxyapatite (HAp) has been widely used to remove cadmium (Cd) in contaminated water and soils via Cd-Ca substitution. The Cd incorporation into HAp affects its structure; however, the detailed mechanism remains unclear. In this study, a series of Cd-substituted hydroxyapatites were synthesized and characterized with various techniques. Cd incorporation causes a decrease in *a*- and *c*-lattice parameters due to the radius of Cd<sup>2+</sup> being slightly smaller than that of Ca<sup>2+</sup>. As the Cd content increases, the particle sizes of the synthesized samples decrease and their specific surface areas increase. Raman bands shift linearly and the  $\nu_1(\text{PO}_4)$  peak at 961 cm<sup>-1</sup> becomes broadened with increasing Cd content. Change in X-ray absorption near edge structure (XANES) spectra of the P *K*-edge indicates distortion of phosphate with Cd incorporation. Total electron yield (TEY) spectra of the Ca *L*<sub>2,3</sub>-edge show a decrease in the octahedral symmetry, suggesting preferential occupancy of Cd over the Ca2 site. Extended X-ray absorption fine structure (EXAFS) analysis of the Ca *K*-edge reveals no obvious change in the local environment of Ca induced by Cd incorporation. However, EXAFS analysis of the Cd *K*-edge indicates that the substituted Cd occupies one Ca2 site in hexagonal Ca2 positions at low-Cd contents [ $<10$  mol% of Cd/(Cd+Ca)], while both Ca1 and Ca2 sites are occupied at higher Cd contents. This study provides atomistic insight into the mechanism for Cd incorporation in HAp, which will help develop an approach for effective Cd removal using HAp for environmental remediation.

**Keywords:** Hydroxyapatite (HAp), cadmium, EXAFS, Raman, incorporation mechanism

### INTRODUCTION

Hydroxyapatite [HAp, Ca<sub>10</sub>(PO<sub>4</sub>)<sub>6</sub>(OH)<sub>2</sub>] is one of the most common apatite-group minerals in nature, particularly important in biological systems, such as bones, teeth, and fossils (Wilson et al. 1999). HAp is also crucial in biological mineralization processes and controls the geochemical cycle of P in soils and sediments (Goldhammer et al. 2010; Zhang et al. 2010). Natural apatites commonly contain foreign cations and/or anions substituted in the crystal structures because of their remarkable tolerance to structural distortion, making apatite-group minerals extremely diverse in chemical composition. Many common cations and anions have been shown to be incorporated into HAp, such as Mg<sup>2+</sup>, Sr<sup>2+</sup>, Mn<sup>2+</sup>, Cd<sup>2+</sup>, CO<sub>3</sub><sup>2-</sup>, SiO<sub>4</sub><sup>4-</sup>, Cl<sup>-</sup>, and F<sup>-</sup> (Hughes and Rakovan 2015; Kim et al. 2017; Pan and Fleet 2002). Among these substitutions, a large number of divalent cations have been reported to occupy Ca sites and alter the structure and properties of HAp, such as lattice parameters (Hughes and Rakovan 2015; Lala et al. 2015; Pan and Fleet 2002). Several cations can even form a complete solid solution of HAp (Pan and Fleet 2002). This characteristic of HAp may lead to its potential environmental applications because the incorporation of toxic metals into HAp structure could fix the metals in the solid phase, thus achieving long-term remediation (Bailey et al. 2005).

Cadmium (Cd) is highly toxic and is a carcinogen harmful to human health. It can be taken in human body through drinking water and nutrition and retain in bones by replacing Ca in hydroxyapatite, which commonly causes serious “Itai-itai” disease (Kobayashi 1978; McLaughlin and Singh 1999). In nature, Cd usually diffuses into soils and water via atmospheric deposition, phosphate fertilizers, and sewage sludge application, causing serious Cd contamination (McLaughlin and Singh 1999). Ca phosphate, especially HAp, is commonly used to remove heavy metals from contaminated water and soils (Bailey et al. 2005; da Rocha et al. 2002; Peld et al. 2004; Srinivasan et al. 2006; Wang et al. 2019; Xu et al. 1994). Cd can co-precipitate with Ca phosphate via isomorphic substitution, which is normally more effective than surface adsorption (Bailey et al. 2005; Valsami-Jones et al. 1998). Furthermore, phosphate has been widely used as a fertilizer for plants in soils, leading to precipitation of Cd-bearing Ca phosphate in soils (McLaughlin and Singh 1999). Thus, mixing phosphate with metal-contaminated soils to form metal-Ca phosphate has been well established as an in situ technique for environmental remediation (Lee et al. 2018; Skwarek and Janusz 2016). In addition, in many phosphate ores, Cd was commonly found to be incorporated in apatite structures (Sery et al. 1996). Understanding the mechanism of Cd incorporation into HAp helps us to understand Cd geochemical behavior and to apply HAp in Cd remediation.

HAp possesses a hexagonal structure with space group *P6<sub>3</sub>/m*

\* E-mail: xcljun@nju.edu.cn

(Kay et al. 1964). HAp has two nonequivalent Ca sites: Ca1 is nine O coordinated (six Ca-O lengths of <2.55 Å and three more distant), while Ca2 is surrounded by seven O atoms with six from five phosphates and one hydroxyl O atom (Online Materials<sup>1</sup> Fig. OM1) (Laurencin et al. 2011; Sery et al. 1996). The molar

ratio of Ca1 to Ca2 is 2:3; thus the chemical formula of HAp can be written as  $\text{Ca}_{14}\text{Ca}_2(\text{PO}_4)_6(\text{OH})_2$  (Zilm et al. 2016; Zougrou et al. 2016). However, the preferred Ca site for cation substitution and associated incorporation mechanism remain unclear.  $\text{Cd}^{2+}$  can occupy all Ca sites in HAp and form complete solid-solutions from  $\text{Ca}_{10}\text{Cd}_0(\text{PO}_4)_6(\text{OH})_2$  to  $\text{Ca}_0\text{Cd}_{10}(\text{PO}_4)_6(\text{OH})_2$  due to their similar radii (Bigi et al. 1986; Lanfranco et al. 2003; Pan and Fleet 2002; Zhu et al. 2016). Thus, Cd atoms may occupy both Ca1 and Ca2 sites in HAp (Hata et al. 1978), and the substituted sites change from one Ca site to both sites as the Cd content increases (Zhu et al. 2016). However, the concentration of Cd in soils or phosphate ores is commonly insufficient to form pure Cd end-member of HAp, and only Cd-bearing Ca-HAp can be found (Bailey et al. 2005; Sery et al. 1996). Thus, understanding the site preference of Cd incorporation into HAp may provide insight into the occurrence of Cd in phosphate-treated Cd-contaminated soils.

The occurrence of Cd in HAp has been investigated by numerous techniques, but the distribution of Cd at Ca1 and Ca2 sites is still a matter of debate. An extended X-ray absorption fine structure (EXAFS) analysis indicates that Cd in apatite from phosphate ores occupies both Ca sites with a slight preference for the Ca2 site (Sery et al. 1996). However, other studies based on X-ray diffraction (XRD) and EXAFS analysis suggest that Cd occurs at both Ca sites without any site preference even at low-Cd concentrations and disclose a linear correlation between lattice parameters and Cd content (Bailey et al. 2005; Lanfranco et al. 2003). On the other hand, density functional theory calculations show that the Ca2 site is favored due to its more covalent character (Tamm and Peld 2006; Terra et al. 2010). Compared to other incorporated ions, Cd has a similar radius to Ca, resulting in small changes in lattice parameters (*a* and *c* from 9.42 and 6.86 Å to 9.32 and 6.65 Å, respectively, for Ca and Cd end-members of HAp) (Lanfranco et al. 2003). Additionally, most EXAFS analyses have only been conducted on Cd without considering the local environment of Ca in HAp, which is also related to the occupied site preference. In this study, we synthesized Cd-substituted HAp with molar ratios of Cd/(Cd+Ca) up to 0.2, conducted both Ca and Cd *K*-edge EXAFS analyses, and obtained total electron yield (TEY) spectra of the Ca  $L_{2,3}$ -edge and X-ray absorption near edge structure (XANES) spectra of the P *K*-edge. The goal was to determine the effects of Cd incorporation on the local atomic environment of Ca and P in HAp and to reveal the mechanism of its Cd incorporation.

## MATERIALS AND METHODS

### Synthesis of HAp and Cd-substituted HAp samples

HAp and Cd-substituted HAp (Cd-HAp) samples were synthesized according to the method of Matsunaga et al. (2010), with dropwise addition of 0.1 M  $(\text{NH}_4)_2\text{HPO}_4$  solution to a mixed solution of 0.1 M  $\text{Ca}(\text{NO}_3)_2 \cdot 4\text{H}_2\text{O}$  and 0.1 M  $\text{Cd}(\text{NO}_3)_2$ . The Cd/(Cd+Ca) molar ratio of the mixed solution varied from 0.01 to 0.20, while the (Ca+Cd)/P ratio was maintained at the stoichiometric ratio of 1.67.

**TABLE 1.** Chemical compositions and refined lattice parameters

Sample	Initial Cd/(Cd+Ca) (mol%) in solution	Cd/(Cd+Ca) (mol%) in solid	(Cd+Ca)/P in solid	SSA ( $\text{m}^2/\text{g}$ )	<i>a</i> (Å)	<i>c</i> (Å)	<i>V</i> (Å <sup>3</sup> )
HA	0	0.00	1.66	86.1	9.426(2)	6.868(2)	528.44(20)
HA-1Cd	1	1.00	1.68	98.0	9.424(2)	6.864(1)	527.96(18)
HA-5Cd	5	4.79	1.68	100.9	9.412(2)	6.852(1)	525.72(18)
HA-10Cd	10	9.14	1.69	113.8	9.402(1)	6.837(1)	523.36(15)
HA-20Cd	20	16.18	1.66	104.6	9.394(1)	6.824(1)	521.51(11)

The pH of the reaction system was kept at 10 by continuously adding an ammonia solution. Obtained precipitates were aged for 48 h, then washed with distilled water, centrifuged, and dried at 60 °C for 24 h. According to initial Cd/(Cd+Ca) ratios of mixed solutions, the synthesized samples were named HAp, HAp-1Cd, HAp-5Cd, HAp-10Cd, and HAp-20Cd (Table 1).

### Sample characterization

The precipitates were characterized using synchrotron X-ray diffraction (XRD) at an incident energy of 18 keV with a wavelength of 0.6883 Å at beamline 14B of the Shanghai Synchrotron Radiation Facility (SSRF). XRD patterns were recorded in the 2θ range of 3–45° using a line-detector model (Yang et al. 2015). Lattice parameters were refined with the GSAS software (Larson and Von Dreele 2000) and EXPGUI interface (Toby 2001). Initial unit-cell parameters for HAp were taken from Hughes et al. (1989).

The Ca, Cd, and P contents of the synthesized HAp samples were determined as follows: 10 mg of each Cd-HAp sample was digested in 10 mL of 2 M  $\text{HNO}_3$  solution, and then Ca, Cd, and P concentrations of the solution were measured by inductively coupled plasma optical emission spectrometry (ICP-AES, Thermo-Fisher Scientific 6300). The morphology of pure HAp and Cd-HAp samples (HAp-10Cd) was characterized with a high-resolution transmission electron microscope (HR-TEM, FEI TF20) operated at 200 kV acceleration voltage. Specific surface areas (SSA) were obtained using the multipoint BET method based on nitrogen adsorption isotherms with a *p/p*<sub>0</sub> range of 0.05–0.20 at 77 K, which were measured on a Micrometrics ASAP 2020 apparatus after degassing at 80 °C for at least 10 h. Raman spectra from 100 to 1400  $\text{cm}^{-1}$  with a resolution of 0.5  $\text{cm}^{-1}$  were collected at room temperature under a 50W×objective of a JY/Horiba LabRAM HR Raman system with a 532.11 nm laser excitation and an 1800-groove/mm grating. Each spectrum was collected with five accumulations to improve the signal-to-noise ratio.

TEY spectra of the Ca  $L_{2,3}$ -edge were collected in the total electron yield mode at beamline 08U1A of SSRF. Sample powders were dispersed on an aluminum foil with a plastic support. The Ca  $L_{2,3}$ -edge spectra were acquired at an energy step of 0.1 eV with three averages per spectrum (Zhang et al. 2015). XANES spectra of the P *K*-edge and EXAFS spectra of the Ca *K*-edge of the synthesized samples were collected at beamline 16A1 of the National Synchrotron Radiation Research Center (NSRRC, Taiwan), with an electronic storage ring of 1.5 GeV and an operating current of 360 mA. EXAFS data for the Cd *K*-edge of Cd-HAp samples were collected at beamline 01C1 of NSRRC. EXAFS data were processed using the Athena and Artemis from the IFEFFIT software package (Ravel and Newville 2005). Backscattering phase and amplitude functions were calculated with FEFF 7.02 (Ankoudinov 1996) from the structure of HAp (Hughes et al. 1989) for Ca spectra and partial Cd-for-Ca substitution for Cd spectra. Multiple scattering effects were neglected for simplification, as adopted in previous analyses of Ca and Cd *K*-edge EXAFS spectra (Bailey et al. 2005; Harries and Hukins 1986; Lanfranco et al. 2003; Laurencin et al. 2011).

## RESULTS

### Characterization of the mineral phases

The Ca, Cd, and P contents of the synthesized samples (Table 1) indicate that (Cd+Ca)/P molar ratios in all HAp samples are almost equal to the stoichiometric ratio of 1.67, and their Cd/(Ca+Cd) molar ratios are similar to those of solutions, except for HAp-20Cd, in which the Cd content is only 16.18 mol%. XRD patterns (Fig. 1a) of all pure HAp and Cd-HAp samples exhibit diffraction peaks of HAp, and no other phases are present. Differences in the peak position, intensity, and full-width at half maximum (FWHM) of (002) are shown in Figure 1b with

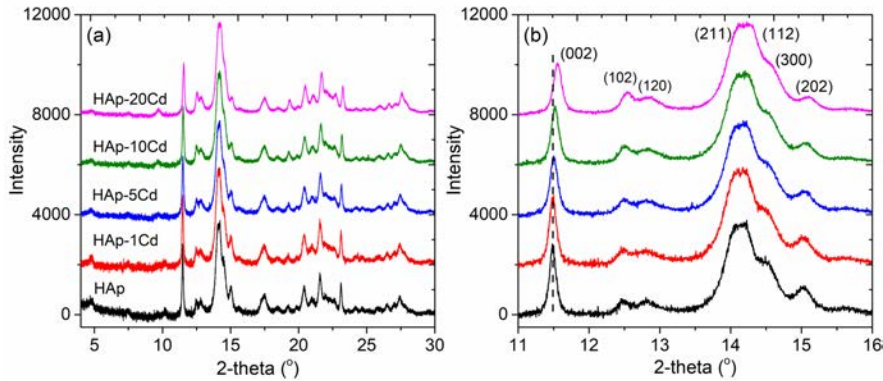


FIGURE 1. Synchrotron XRD patterns of pure HAp and Cd-HAp samples. (Color online.)

an enlarged XRD pattern in the range of  $11^\circ \leq 2\theta \leq 16^\circ$ , which clearly shows the shift of peak (002) to smaller  $d$ -spacing values and broader FWHM values with increasing Cd content (Online Materials<sup>1</sup> Fig. OM2). The shift is not obvious in HAPs with low-Cd contents (HAp-1Cd and HAp-5Cd) because of the similarity between the radii of  $\text{Cd}^{2+}$  (0.095 nm) and  $\text{Ca}^{2+}$  (0.100 nm) (Shannon 1976). Lattice parameters  $a$  and  $c$  decrease slightly from 9.426 and 6.868 Å to 9.394 and 6.824 Å, respectively (Table 1), which are linearly correlated with Cd content (Online Materials<sup>1</sup> Fig. OM3), indicating homogenous substitution (Lanfranco et al. 2003; Srinivasan et al. 2006; Terra et al. 2010). The decrease in the intensity of peak (002) and the broadening in its peak width with increasing Cd content indicate a decline in the degree of crystallization.

TEM images (Fig. 2) show that all the synthesized HAP samples have spindle shapes, consistent with reported HAP

crystals (Lowry et al. 2017). With an increase of Cd content in HAP, the particle sizes decrease from 50–60 nm (HAP) to <30 nm (HAp-10Cd), which explains the increase in SSA from 86.1 m<sup>2</sup>/g (HAP) to 113.8 m<sup>2</sup>/g (HAp-10Cd) (Table 1). The interplanar (002) spacing in HR-TEM images also decreases from 3.458 to 3.446 Å (Figs. 2b and 2e), which is consistent with the (002) XRD peak's shifting to higher  $2\theta$  values (Online Materials<sup>1</sup> Fig. OM2). Selected-area electron diffraction (SAED) patterns (Figs. 2c and 2f) show that the (221) and (222) planes have strong diffraction intensities.

#### Raman spectra and P *K*-edge XANES spectra of synthesized HAPs

Local distortions of phosphate in the HAP structure induced by Cd incorporation are investigated by Raman spectroscopy and XANES analysis. Normalized Raman spectra of pure HAP

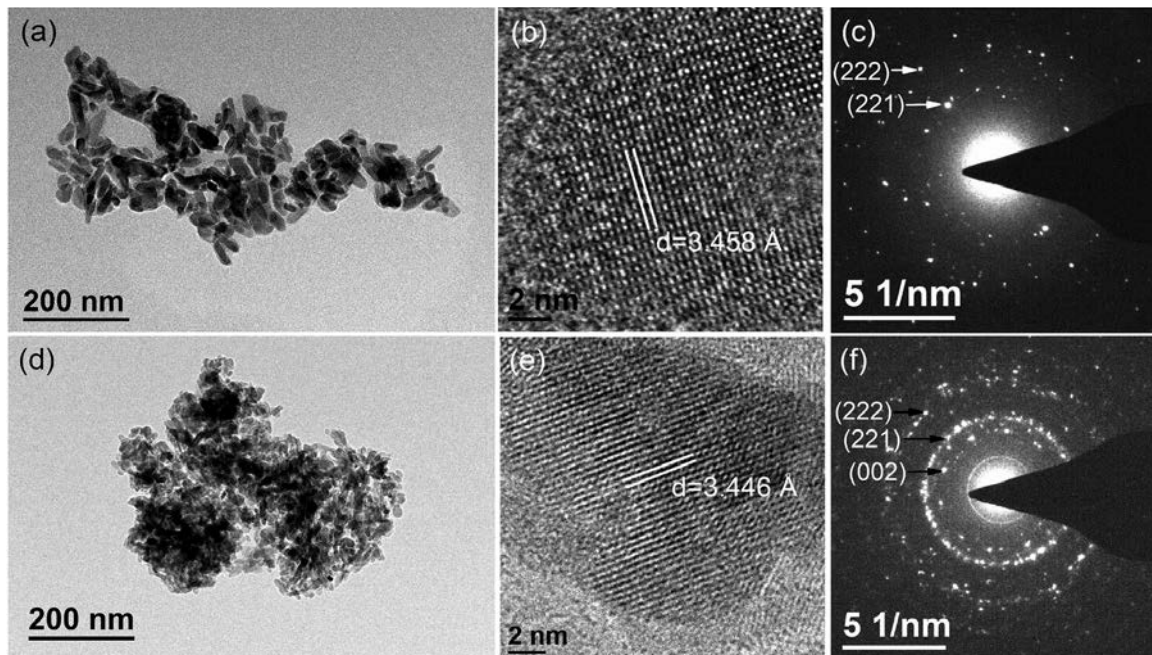
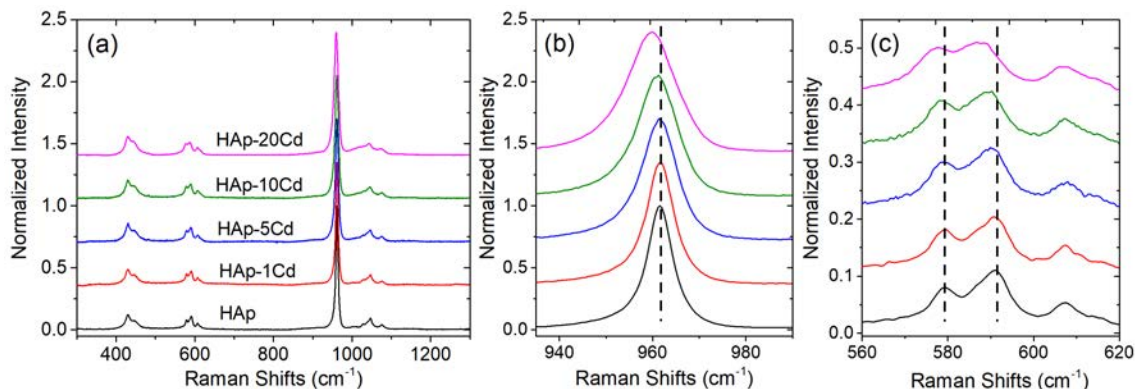


FIGURE 2. TEM images of pure HAp (a, b, and c) and HAp-10Cd (d, e, and f). (f) displays bright rings from the SAED area (200 nm) that contains many crystals due to their small sizes.



**FIGURE 3.** Raman spectra of pure HAp and Cd-HAp samples (a) and the magnified Raman spectra in wavenumbers of 940–990  $\text{cm}^{-1}$  (b) and 560–620  $\text{cm}^{-1}$  (c). The highest intensities of all spectra are normalized to be 1.0 for better comparison. (Color online.)

and Cd-HAp samples (Fig. 3a) and peak positions are consistent with typical bands of the HAp phase, and mode assignments are compiled in Online Materials<sup>1</sup> Table OM1 (Antonakos et al. 2017; Guerra-López et al. 2015). For all samples, the strong peak at 961  $\text{cm}^{-1}$  has been assigned to the symmetric  $\nu_1$  stretching vibration of  $\text{PO}_4$  groups, and peaks of three  $\nu_3(\text{PO}_4)$ , three  $\nu_4(\text{PO}_4)$ , and two  $\nu_2(\text{PO}_4)$  vibrations are also observed. The peak position of  $\nu_1(\text{PO}_4)$  shifts slightly down to lower wavenumbers (Fig. 3b), and the FWHM values increase from 6.6 to 12.9  $\text{cm}^{-1}$  with increasing Cd content (Online Materials<sup>1</sup> Table OM1), showing linear correlations with substituted Cd (Online Materials<sup>1</sup> Fig. OM4). In particular, as the Cd content increases, three peaks at ~579, 591, and 607  $\text{cm}^{-1}$  assigned to  $\nu_4(\text{PO}_4)$  vibrations exhibit a redshift and the intensity ratio of the two peaks at 579 and 591  $\text{cm}^{-1}$  increases (Fig. 3c). All of these changes indicate an increase in progressive distortion of the tetrahedral phosphate unit with Cd incorporation (Antonakos et al. 2007; Petit et al. 2017).

The P *K*-edge XANES spectra of pure HAp and Cd-HAp samples present the features of four peaks, consistent with the reported HAp phase (Online Materials<sup>1</sup> Fig. OM5) (Liu et al. 2017). For all Cd-HAp samples, an edge jump (peak 1), a shoulder (peak 2), and two post-edge peaks (3 and 4) are at the same energy positions, exhibiting the same Ca-bound P environment (Prietz et al. 2013). However, the intensity of the shoulder related to peak 1 decreases slightly and progressively. This behavior implies an increased structural disorder of HAp with increasing Cd content, likely induced by the  $\text{PO}_4$  groups bound with substituted Cd (Prietz et al. 2013).

#### Ca $L_{2,3}$ -edge TEY spectra of synthesized HAp

The energy positions of the main  $L_3$  ( $a_2$  at ~349.4 eV) and  $L_2$  peaks ( $b_2$  at ~352.7 eV), as well as pre-edge peaks (hereafter called  $a_1$  and  $b_1$ ) in the Ca  $L_{2,3}$ -edge TEY spectra of all HAp samples (Fig. 4) are quite similar. Commonly, the split energy of  $a_1$  and  $a_2$  peaks is proportional to the crystallinity of HAp (Beniash et al. 2009; Politi et al. 2008; Zougrou et al. 2016). The split energy of pure HAp and Cd-HAp are similar to each other (Online Materials<sup>1</sup> Fig. OM6 and Table OM2), indicating little change in the crystallinity due to Cd incorporation, which is also consistent with XRD results. For pre-edge peaks,  $a_1$  has

been reported to represent the octahedral ( $O_h$ ) symmetry of  $\text{Ca}^{2+}$  caused by the 2p-3d spin-orbit coupling, mainly contributed from Ca2 sites (Cosmidis et al. 2015; Naftel et al. 2001). The decrease in relative intensities ( $a_1/L_3$  in Online Materials<sup>1</sup> Table OM2) with Cd content indicates that the  $O_h$  symmetry from the Ca2 site decreases with Cd incorporation, suggesting that Cd has preferentially entered this site. This interpretation relies on the assumption that the coordination environment (coordination numbers and bond distance) of Ca in each site remains the same upon Cd incorporation (Laurencin et al. 2011). Given that the local environment of Ca mainly depends on the  $\text{Ca}\cdots\text{O}$  coordination, the average bond distances and coordination numbers of  $\text{Ca}\cdots\text{O}$  in the first spheres should be similar for all HAp samples. To confirm this interpretation, EXAFS spectra of the Ca *K*-edge are analyzed to reveal the local environment of Ca.

#### EXAFS spectra of the Ca *K*-edge in HAp

The Ca *K*-edge XANES spectra of Cd-HAp samples are nearly identical to that of pure HAp, except for a decrease in the shoulder peak intensity (Online Materials<sup>1</sup> Fig. OM7a). The XANES spectrum of HAp-20Cd with the highest Cd content is nearly identical to that of pure HAp (Online Materials<sup>1</sup> Fig. OM7b), especially in the pre-edge region, which is sensitive to

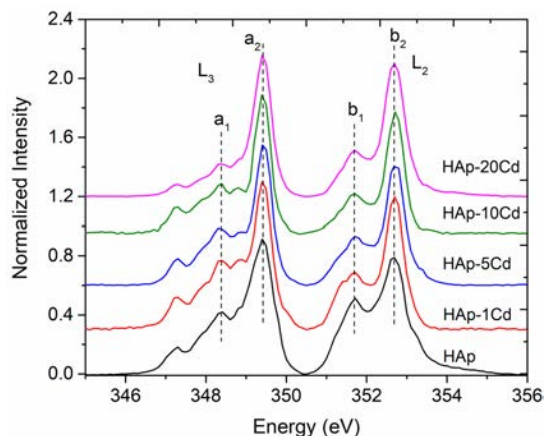


**FIGURE 4.** TEY spectra of the Ca  $L_{2,3}$ -edge in pure HAp and Cd-HAp samples. (Color online.)

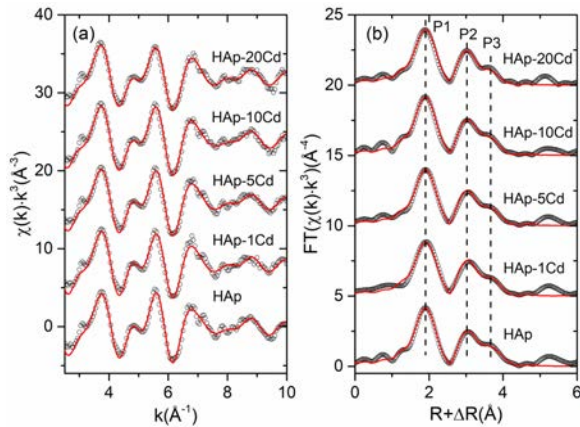


**FIGURE 5.** EXAFS spectra of  $k^3$ -weighted (a) and Fourier transform magnitudes (b) of the Ca  $K$ -edge in pure HAp and Cd-HAp samples. Dots are raw data, and solid lines are their structural fits. (Color online.)

the local distortion around Ca cations. The pre-edge region at 4037 eV due to the  $1s \rightarrow 3d$  electron transition is similar regardless of Cd content, suggesting that the local environments of Ca are similar in Cd-HAp samples (Laurencin et al. 2011; Neuvillle et al. 2004).

EXAFS spectra of the Ca  $K$ -edge and their structural fitting of HAp samples are shown in Figure 5 and listed in Online Materials<sup>1</sup> Table OM3. The  $k^3\chi(k)$  spectra and the Fourier transforms (FT) of HAp and Cd-HAps are very similar, consistent with the

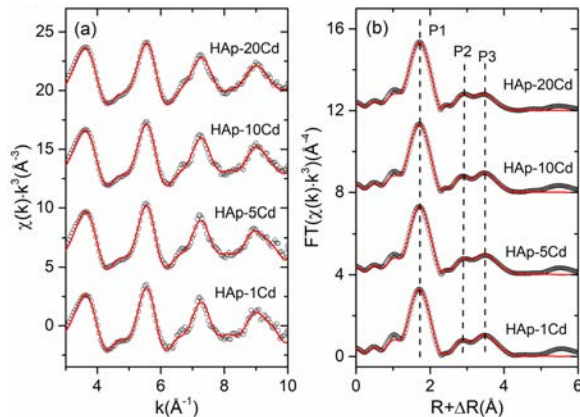


**FIGURE 6.** EXAFS spectra of  $k^3$ -weighted (a) and Fourier transform magnitudes (b) of the Cd  $K$ -edge of Cd-HAp samples. Dots are raw data, and solid lines are their structural fits. (Color online.)

reported HAp spectra (Harries and Hukins 1986; Harries et al. 1988; Laurencin et al. 2011). Their Fourier transforms show three peaks with similar intensities of the first peak at  $\sim 1.9 \text{ \AA}$  (indicated by P1 and not corrected for phase shifts) (Fig. 5b), and the fitted bond distances and Debye-Waller factors ( $\sigma^2$ ) are quite similar, suggesting that the local geometry of the nearest  $\text{Ca}\cdots\text{O}$  shell is not significantly modified by Cd incorporation. For distant shells ( $>3 \text{ \AA}$ ) contributed from the backscattering of surrounding P, Ca, and more distant O (Harries and Hukins 1986; Laurencin et al. 2011), neither the spectra nor fitting results show any noteworthy change due to Cd incorporation. For HAp-20Cd, the third peak (P3) is slightly stronger than that in HAp (Fig. 5b). Given that this part of the spectrum arises from Ca atoms, the increase in the P3 intensity may result from the presence of Cd atoms, which are heavier and thus have stronger backscattering than Ca. However, it is difficult to evaluate any change in the long-range ordering around Ca due to slight differences among fitting parameters (Online Materials<sup>1</sup> Table OM3). The low-Cd content and similar ion radii of  $\text{Cd}^{2+}$  and  $\text{Ca}^{2+}$  hardly modify the local environment of Ca.

### EXAFS spectra of the Cd $K$ -edge in HAps

There is no perceptible change due to Cd incorporation in XANES spectra of the Cd  $K$ -edge in Cd-HAp samples (Online Materials<sup>1</sup> Fig. OM8), implying that the local geometries are similar regardless of Cd content in HAps. The EXAFS spectra and structural fitting results for Cd in HAp samples are shown in Figure 6 and Table 2. The Fourier transforms of  $k^3\chi(k)$  in R-space also exhibit three main peaks (Fig. 6b), displaying that peak 1 (P1) is identical while there are a small but systematic increase in peak 2 (P2) and a decrease in peak 3 (P3). In comparison with the Ca  $K$ -edge spectra of pure Ca-HAp (Fig. 5b), peak 2 in the Cd  $K$ -edge spectra is more intense than peak 3. In pure Ca-HAp, peak 2 results from the contribution of  $\text{Ca}\cdots\text{P}$  (3rd shell) and  $\text{Ca}\cdots\text{Ca}$  (4th shell) backscattering, which are mainly derived from Ca1 as the center atom (Online Materials<sup>1</sup> Table OM3) (Laurencin et al. 2011). In low-Cd-HAp samples (HAp-1Cd, HAp-5Cd, and HAp-10Cd), peak 2 is relatively weak, indicating that Cd is located at the Ca2 site with only three P shells backscattering contributing to the low intensity of peak 2 (Lanfranco et al. 2003). However, in HAp-20Cd, the increase in the peak 2 intensity indicates that the backscattering from Cd at the Ca1 site also contributes to this peak because Cd1 in Cd-HAp has the shortest  $\text{Cd}\cdots\text{Ca}$  distance (Harries and Hukins 1986). This also confirms that in the Cd-HAp end-member, Cd occupies all Ca1 and Ca2 sites, and EXAFS spectra of the Cd  $K$ -edge are similar to those of the Ca  $K$ -edge in both Ca- and Cd-HAp end-members, with

**TABLE 2.** Fitting parameters of the Cd  $K$ -edge EXAFS spectra of Cd-HAp samples with the model of Cd at the Ca2 site

Atom/Shell	HAp-1Cd			HAp-5Cd			HAp-10Cd			HAp-20Cd		
	N <sup>a</sup>	R (Å)	$\sigma^2(10^{-3}\text{nm}^2)$									
O/1st	5	2.28	0.008	5	2.29	0.008	5	2.28	0.009	5	2.28	0.009
O/2nd	2	2.52	0.015	2	2.52	0.014	2	2.51	0.017	2	2.51	0.023
P/3rd	1	3.08	0.006	1	3.08	0.008	1	3.08	0.008	1	3.08	0.010
P/4th	2	3.38	0.025	2	3.37	0.028	2	3.42	0.032	2	3.37	0.028
P/5th	2	3.78	0.030	2	3.74	0.030	2	3.79	0.030	2	3.67	0.030
Ca/6th	6	3.97	0.010	6	3.98	0.011	6	3.97	0.013	6	3.96	0.015
Ca/7th	4	4.15	0.005	4	4.16	0.006	4	4.14	0.008	4	4.13	0.011

Note: Typical errors on the bond distances and Debye-Waller factors are  $\pm 0.02 \text{ \AA}$  in R and 20% in  $\sigma^2$ , respectively.

<sup>a</sup> Values fixed at averaged crystallographic values.

a stronger peak 2 than peak 3 (Sery et al. 1996). Thus, because of the weaker intensity of peak 2 than that of peak 3 in Cd-HAp, we deduce that Cd preferentially occupies the Ca2 site in HAp at a low content, and the structural fittings of the spectra of Cd-HAps are conducted with Cd at the Ca2 site.

The fitting parameters listed in Table 2 show that peak 1 derived from two Cd···O shells displays the shortest Cd-O distance of 2.28 Å, which is consistent with the reported shortest Ca-O distance of Ca2 sites in pure Ca-HAp (Harries and Hukins 1986). The fitting parameters of the bond distance and Debye-Waller factor ( $\sigma^2$ ) are quite similar for HAp-1Cd, HAp-5Cd, and HAp-10Cd. The good fit assuming that Cd is located at the Ca2 site confirms that Cd incorporates into the Ca2 site preferentially. However, the difference in the fifth shell of Cd···P in HAp-20Cd has a shorter bond distance of 3.67 Å, which is much shorter than those of HAps with low-Cd contents. Since Cd at the Ca1 site has been reported to have a shorter Cd1···P distance (Laurencin et al. 2011), the backscattering of the surrounding P of Cd1 could make the fitted distance shorter. This may also result in an increase in the peak 2 intensity, suggesting that Cd atoms also occupy Ca1 sites in HAps with high-Cd contents.

## DISCUSSION

### Effect of Cd incorporation on the HAp crystal structure

The linear decreases in lattice parameters ( $a$ ,  $c$ , and  $V$ ) with substituted Cd content mainly result from the smaller radius of Cd<sup>2+</sup> compared with Ca<sup>2+</sup> (Bigi et al. 1986; Lanfranco et al. 2003). The decrease in intensity and the increase in width of the XRD peak (002) (Online Materials<sup>1</sup> Fig. OM2) indicate slightly decreased crystallinity due to Cd incorporation (Zhu et al. 2016). In contrast, several synthesized metal-substituted HAps with Mg<sup>2+</sup> and Zn<sup>2+</sup> suggest that the crystallinity of substituted HAps decreases obviously at 5 and 10% substitutions (Arul et al. 2018; Guerra-López et al. 2015), as both Mg<sup>2+</sup> and Zn<sup>2+</sup> have much smaller radii than Ca<sup>2+</sup> ( $r_{\text{Mg}^{2+}} = 0.72$  Å,  $r_{\text{Zn}^{2+}} = 0.74$  Å, and  $r_{\text{Ca}^{2+}} = 1.00$  Å). Interestingly, sorption experiments of Cd<sup>2+</sup> and Zn<sup>2+</sup> on HAp also indicate that Cd<sup>2+</sup> may be more easily incorporated into the HAp structure than Zn<sup>2+</sup> (Xu et al. 1994).

Changes in the local environment of phosphate in HAps due to Cd incorporation are reflected by modifications of peak position, FWHM, and the intensity of Raman spectra. The redshift and broadening of  $\nu_1(\text{PO}_4)$  are linearly correlated with Cd content. The  $\nu_1(\text{PO}_4)$  mode was reported to correspond with the vibration in which P, O1, and O2 atoms are on the mirror plane and two O3 atoms are at both sides of the plane (Antonakos et al. 2007). The incorporated Cd at the Ca2 site is bound with two next-nearest O3 atoms, producing a distortion of phosphate with a slight decrease in the O3-P-O3 angle due to the smaller radius of Cd and the mass difference (Hata et al. 1978; Mercier et al. 2005). The distortion of phosphate bound with Cd results in redshifts and broadening of  $\nu_1(\text{PO}_4)$ , where both of them exhibit a linear relation with Cd content. The substitution of other cations in HAp was also reported to cause phosphate distortions and induce a change in Raman spectra (Antonakos et al. 2007, 2017; Stammer et al. 2018; Terra et al. 2009). For other substituted cations, in comparison, a 3.2 mol% Zn substitution could cause a shift of 2 cm<sup>-1</sup>, while the incorporated Cd with a content of 16.18 mol%

only induces a 2 cm<sup>-1</sup> shift, indicating that the effect of Cd<sup>2+</sup> incorporation on the symmetry distortion of phosphate tetrahedron is much weaker than Zn<sup>2+</sup> due to similar radii of Ca<sup>2+</sup> and Cd<sup>2+</sup> (Guerra-López et al. 2015; Lanfranco et al. 2003). Such effects of Cd incorporation are also reflected by the decline in  $\nu_3(\text{PO}_4)$  peaks at 1025, 1045, and 1073 cm<sup>-1</sup> (Antonakos et al. 2017). However, the change induced by Cd incorporation is too slight to alter the bond length of P-O even as the Cd content reaches 16.18 mol%. In that case, the slight change only causes a small decrease in the shoulder peak (peak 2 in Online Materials<sup>1</sup> Fig. OM5) of the P K-edge XANES spectra, and the P K-edge XANES analysis might not be sensitive enough to differentiate the crystallinity of HAp with Cd incorporation (Chen and Arai 2019). The small difference between the ionic radii of Ca<sup>2+</sup> and Cd<sup>2+</sup> (only 0.04 Å) only changes the structure slightly without disrupting the framework, which also contributes to the thermodynamic basis to form completely continuous solid-solutions of Ca<sub>10</sub>(PO<sub>4</sub>)<sub>6</sub>(OH)<sub>2</sub>-Cd<sub>10</sub>(PO<sub>4</sub>)<sub>6</sub>(OH)<sub>2</sub> (Pan and Fleet 2002).

### Site preference of Cd incorporation into HAp

Ca1 and Ca2 are crystallographically distinct sites in HAp, and both have the potential for substitution of foreign ions. Although the preferred Ca site for different foreign ions is still under debate, more studies have suggested that Ca2 is the preferred site based on Rietveld analysis of XRD data and first-principles calculations (Guerra-López et al. 2015; Lala et al. 2015; Luo et al. 2009; Terra et al. 2010). In this study, the local environment of Ca and Cd in HAp are investigated, and the incorporation mechanism is revealed by combining Ca L<sub>2,3</sub>-edge TEY, Ca K-edge EXAFS, and Cd K-edge EXAFS analyses. The surrounding atomistic environment of Ca with O is hardly altered by Cd incorporation (<20 mol%), which has also been confirmed in the Ca K-edge spectra of Mg-substituted HAp (Laurencin et al. 2011). The similarity of the bond distance and coordination number of Ca in Cd-HAps confirms that Cd is indeed at the Ca2 site, as reflected in the Ca L<sub>2,3</sub>-edge TEY spectra. According to Ca L<sub>2,3</sub>-edge TEY spectra (Fig. 4) and EXAFS spectra of the Cd K-edge (Fig. 6b), we propose that Cd atoms prefer to occupy the Ca2 site, and the reasonable fitting of  $r_{\text{Cd-O}} = 2.28$  Å is consistent with the Cd2-O distance (2.28 Å) (Harries and Hukins 1986). The higher electronegativity of Cd (1.7) over Ca (1.0) results in a higher preference of Cd for Ca2 site to increase covalent interactions with the hydroxyl oxygen bonding with Ca2 (Terra et al. 2010). Furthermore, theoretical calculations have shown that Cd at Ca1 sites largely increases variation in the Cd-O distance (Terra et al. 2010), which is opposite to the results of a similar Cd-O distance in EXAFS fitting and a linear decrease in lattice parameters of Cd-HAps with increasing Cd content (Lanfranco et al. 2003). Thus, the Ca2 site in HAp is preferential for Cd incorporation. However, the possible limited content of incorporated Cd that only occupies Ca2 sites needs to be explored.

The spatial accommodation without disrupting the framework should be a key factor to determine the site preference with different Cd contents (Pan and Fleet 2002). From the geometrical configuration of Ca2 atoms in the HAp structure, two adjacent triangles ( $\Delta$ ,  $\times$ ) with the nearest cations are shown to form one Ca2 hexagon (Online Materials<sup>1</sup> Figs. OM9a and OM9b). Occupancy at one Ca2 site in the Ca2 hexagon reaches a Cd content

of 10 mol%. Assuming homogenous substitution of Cd without forming a Cd-Cd cluster in the HAp structure, substituted Cd should first occupy Ca2 sites diagonally with the longest Cd-Cd bond distance in the Ca2 hexagon (Online Materials<sup>1</sup> Fig. OM9c and OM9d), in which the excess energy for the maximized Cd2-Cd2 distance is more negative to favor this configuration (Terra et al. 2010). Thus, Cd atoms occupying two Ca2 sites in one hexagon could reach 20 mol% of all Ca sites in HAp. However, our EXAFS analysis indicates that Cd also occupies Ca1 sites in HAp-20Cd ( $\geq 16.18$  mol%), suggesting that only one Ca2 site in the Ca2 hexagon is preferentially substituted by Cd. Then, with further increasing Cd content above 10 mol%, Cd starts to occupy Ca1 sites after filling one Ca2 site in the Ca2 hexagon. Thus, 10 mol% is a limited Cd content for occupying Ca2 sites only, which is also consistent with theoretical calculation results of excess energies that HAp with 10 mol% Cd has the lowest excess energy with Cd occupying Ca2 sites compared to mixed Ca1/Ca2 sites and Ca1 sites (Terra et al. 2010). Hence, we propose a conceptual model for Cd incorporation in HAp at different Cd contents (Fig. 7). Cd ions first occupy hexagonal Ca2 positions since the Cd content is lower than 10 mol% (Fig. 7a). As the Cd content increases to 10–20 mol%, Cd ions prefer to occupy the Ca1 site after one of the two Ca2 sites in each Ca2 hexagon is occupied (Figs. 7b and 7c). Furthermore, it is deduced that Cd could occupy all Ca2 and Ca1 sites (Fig. 7d) and eventually form the end-member Cd-HAp [ $\text{Ca}_6\text{Cd}_{10}(\text{PO}_4)_6(\text{OH})_2$ ] (Hata et al. 1978; Lanfranco et al. 2003).

The effect of the preferential occupancy of Cd at the Ca2

site may help us understand the change in lattice parameters with Cd incorporation. The decrease of  $a$  and  $c$  parameters has a very good linear relation with increasing Cd content at low-Cd contents (<10 mol%), but shows a smaller decreasing rate at a Cd content of 16 mol% (Online Materials<sup>1</sup> Fig. OM3), which may result from Cd at Ca2 with a low-Cd content and Cd at both Ca1/Ca2 sites with higher Cd contents. It has been reported that pure Cd2 substitution results in smaller lattice parameters  $a$  and  $c$  than pure Cd1 substitution in HAp (Tamm and Peld 2006; Terra et al. 2010). This may explain our observed change in lattice parameters  $a$  and  $c$  where the decrease rate is reduced at higher Cd contents (Online Materials<sup>1</sup> Fig. OM3). With further increasing Cd content to form a complete Ca-Cd solid solution with mixed Cd2/Cd1 substitution, the change in lattice parameters becomes linear with Cd content, as reported in previous studies, in which the increased interval of Cd content is  $\sim 10$  mol% (Lanfranco et al. 2003; Srinivasan et al. 2006; Terra et al. 2010).

The site preference of Cd in HAp also controls the dissolution process of Cd-HAp samples. Previous dissolution experiments show that HAp samples with various Cd contents exhibit different dissolution behaviors because of the preferred Ca sites for Cd (Zhu et al. 2016). Average solubility products ( $K_{sp}$ ) change rapidly from  $10^{-57.65}$  (pure HAp) to  $10^{-59.18}$  (HAp with 8 mol% Cd), but change slowly at higher Cd contents (Zhu et al. 2016). This study provides a novel atomistic explanation that Cd only occupies the Ca2 site (<10 mol%) and alters the kinetics of surface ions release (Terra et al. 2010). The preferred

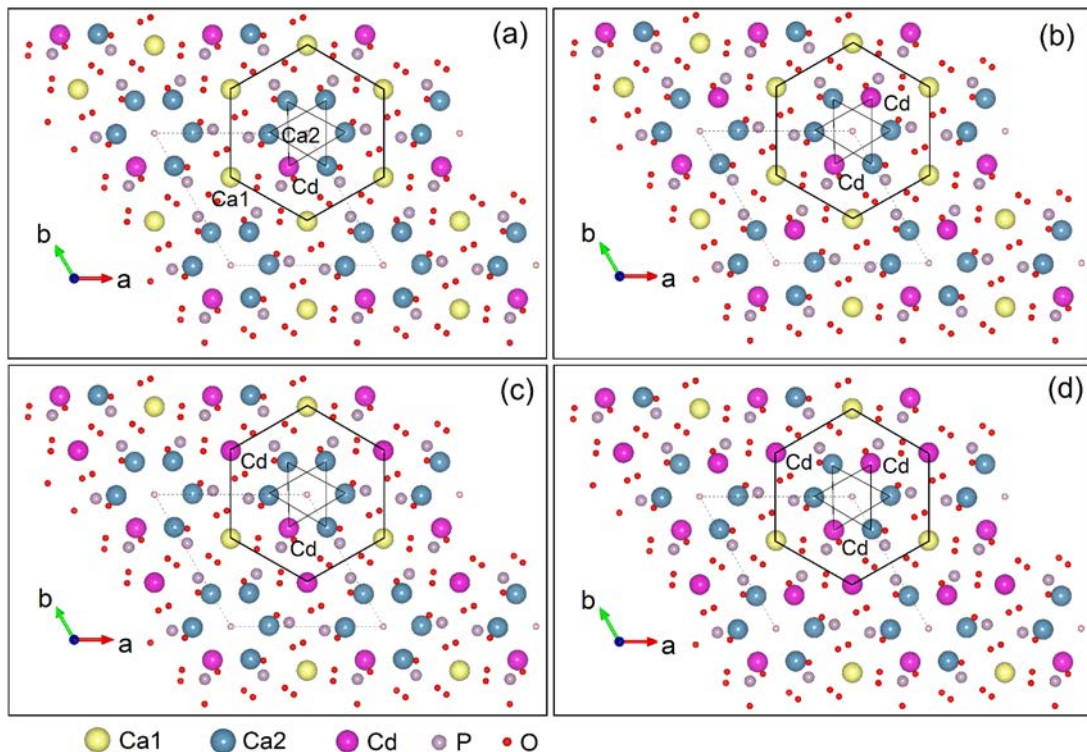


**FIGURE 7.** Representation of Cd incorporation into the HAp structure. (a) Cd in one Ca2 site (<10 mol%); (b) Cd in two Ca2 sites (10–20 mol%); (c) Cd in one Ca2 site and one Ca1 site (10–20 mol%); (d) Cd in two Ca2 sites and one Ca1 site (>20 mol%). (Color online.)

Ca2 site for Cd substitution could enhance Cd retention in the solid phase, as evidenced by sorption experiments, in which the sorption of Cd<sup>2+</sup> on HAp easily triggers coprecipitation of Cd-HAp (Srinivasan et al. 2006; Xu et al. 1994).

### IMPLICATIONS

Cd first occupies one Ca2 site at hexagonal Ca2 positions when the Cd content is lower than 10 mol% and then begins to occupy the Ca1 site with increasing Cd content. The Cd incorporation only slightly changes the HAp long-range structure but increases local structural disorder. As reported previously, Cd could diffuse into HAp during Cd sorption by HAp and form Cd-substituted HAp (Bailey et al. 2005; Xu et al. 1994). This study demonstrates that the incorporated Cd affects the HAp structure less than other metals (e.g., Zn<sup>2+</sup>), revealing that the employment of HAp for Cd removal in contaminated water and soils may be effective. Natural soils and water only contain trace amounts of Cd [commonly <500 mg/kg (McLaughlin and Singh 1999)], and the preferential occupancy of Ca2 via Cd under low-Cd contents could contribute to long-term retention of Cd.

Cation substitutions in various minerals play key roles in geochemical and environmental processes because substituted minerals commonly exhibit characteristics of both ions and modify surface reactivity. Cu-substituted HAp has been reported to enhance arsenate sorption compared to pure HAp (Liu et al. 2010). The increased surface area with Cd substitution suggests a potential improvement in the sorption of toxic elements (e.g., Pb, Zn, As, etc.) by Cd-substituted HAp. Additionally, the formation of solid solutions has been widely employed to remove heavy metals from groundwater and soils and fix these heavy metals in solid phases for long-term remediation. Compared to surface adsorption, Cd incorporation into the HAp structure implies that the Cd release from Cd-substituted HAp must break the HAp framework, suggesting that HAp may be a high-performance material for removing and storing Cd from contaminated environments.

### ACKNOWLEDGMENTS AND FUNDING

We appreciate the constructive comments from Editor Hongwu Xu, Associate Editor Jie Xu, and two anonymous reviewers on early versions. This work is financially supported by National Science Foundation of China (41730316, 41902032, and 41425009). H.L. is also supported by the Fundamental Research Funds for the Central Universities (14380104). We gratefully acknowledge beamlines BL08U1A and BL14B at Shanghai Synchrotron Radiation Facility (SSRF) for providing the beam time for TEY and SR-XRD measurements. We appreciate beamlines BL16A1 and BL01C1 at NSRRC for XANES analysis of P and EXAFS analysis of Ca and Cd. We are also grateful to Jiani Chen, Zhenmeng Sun, Xiaolin Wang, and Ye Qiu for help with the analyses in TEM, BET, and Raman spectra.

### REFERENCES CITED

- Ankoudinov, A.L. (1996) Relativistic Spin-dependent X-ray Absorption Theory. Ph.D. Thesis, University of Washington.
- Antonakos, A., Liarokapis, E., Kyriacou, A., and Leventouri, T. (2017) Raman and IR studies of the effect of Fe substitution in hydroxyapatites and deuterated hydroxyapatite. *American Mineralogist*, 102, 85–91.
- Antonakos, A., Liarokapis, E., and Leventouri, T. (2007) Micro-Raman and FTIR studies of synthetic and natural apatites. *Biomaterials*, 28, 3043–3054.
- Arul, K.T., Ramesh, M., Chennakesavan, C., Karthikeyan, V., Manikandan, E., Umar, A., Maaza, M., and Henini, M. (2018) Novel multifunctional of magnesium ions (Mg<sup>2+</sup>) incorporated calcium phosphate nanostructures. *Journal of Alloys and Compounds*, 730, 31–35.
- Bailey, E.H., Mosselmans, J.F.W., and Young, D. (2005) Time-dependent surface reactivity of Cd sorbed on calcite, hydroxylapatite and humic acid. *Mineralogical Magazine*, 69, 563–575.
- Beniash, E., Metzler, R.A., Lam, R.S.K., and Gilbert, P.U.P.A. (2009) Transient amorphous calcium phosphate in forming enamel. *Journal of Structural Biology*, 166, 133–143.
- Bigi, A., Gazzano, M., Ripamonti, A., Foresti, E., and Roveri, N. (1986) Thermal stability of cadmium-calcium hydroxyapatite solid solutions. *Journal of the Chemical Society, Dalton Transactions*, 241–244.
- Chen, K.-Y., and Arai, Y. (2019) X-ray diffraction and X-ray absorption near-edge structure spectroscopic investigation of hydroxyapatite formation under slightly acidic and neutral pH conditions. *ACS Earth and Space Chemistry*, 3, 2266–2275.
- Cosmidis, J., Benzerara, K., Nassif, N., Tyliczszak, T., and Bourdelle, F. (2015) Characterization of Ca-phosphate biological materials by scanning transmission X-ray microscopy (STXM) at the Ca L<sub>2,3</sub>, P L<sub>2,3</sub>, and C K-edges. *Acta Biomaterialia*, 12, 260–269.
- da Rocha, N.C.C., de Campos, R.C., Rossi, A.M., Moreira, E.L., Barbosa, AdF., and Moure, G.T. (2002) Cadmium uptake by hydroxyapatite synthesized in different conditions and submitted to thermal treatment. *Environmental Science & Technology*, 36, 1630–1635.
- Goldhammer, T., Brüchert, V., Ferdelman, T.G., and Zabel, M. (2010) Microbial sequestration of phosphorus in anoxic upwelling sediments. *Nature Geoscience*, 3, 557–561.
- Guerra-López, J.R., Echeverría, G.A., Güida, J.A., Viña, R., and Punte, G. (2015) Synthetic hydroxyapatites doped with Zn(II) studied by X-ray diffraction, infrared, Raman and thermal analysis. *Journal of Physics and Chemistry of Solids*, 81, 57–65.
- Harries, J.E., and Hukins, D.W.L. (1986) Analysis of the EXAFS spectrum of hydroxyapatite. *Journal of Physics C: Solid State Physics*, 19, 6859–6872.
- Harries, J.E., Hukins, D.W.L., and Hasnain, S.S. (1988) Calcium environment in bone mineral determined by EXAFS spectroscopy. *Calcified Tissue International*, 43, 250–253.
- Hata, M., Okada, K., Iwai, S., Akao, M., and Aoki, H. (1978) Cadmium hydroxyapatite. *Acta Crystallographica Section B Structural Crystallography and Crystal Chemistry*, 34, 3062–3064.
- Hughes, J.M., Cameron, M., and Crowley, K.D. (1989) Structural variations in natural F, OH, and Cl apatites. *American Mineralogist*, 74, 870–876.
- Hughes, J.M., and Rakovan, J.F. (2015) Structurally robust, chemically diverse: apatite and apatite supergroup minerals. *Elements*, 11, 165–170.
- Kay, M.L., Young, R.A., and Posner, A.S. (1964) Crystal structure of hydroxyapatite. *Nature*, 204, 1050–1052.
- Kim, Y., Konecke, B., Fiege, A., Simon, A., and Becker, U. (2017) An ab-initio study of the energetics and geometry of sulfide, sulfite, and sulfate incorporation into apatite: The thermodynamic basis for using this system as an oxybarometer. *American Mineralogist*, 102, 1646–1656.
- Kobayashi, J. (1978) Pollution by cadmium and the itai-itai disease in Japan. In F. W. Oehme, Ed., *Toxicity of Heavy Metals in the Environment*, pp. 199–260, Marcel Dekker, Inc.
- Lala, S., Ghosh, M., Das, P.K., Kar, T., and Pradhan, S.K. (2015) Mechanical preparation of nanocrystalline biocompatible single-phase Mn-doped A-type carbonated hydroxyapatite (A-cHAp): Effect of Mn doping on microstructure. *Dalton Transactions Dalton Transactions* 44(46), 20087–20097.
- Lanfranco, A.M., Schofield, P.F., Murphy, P.J., Hodson, M.E., Mosselmans, J.F.W., and Valsami-Jones, E. (2003) Characterization and identification of mixed-metal phosphates in soils: the application of Raman spectroscopy. *Mineralogical Magazine*, 67, 1299–1316.
- Larson, A.C., and Von Dreele, R.B. (2000) General Structure Analysis System (GSAS). Los Alamos National Laboratory Report LAUR, 86-748.
- Laurencin, D., Almora-Barrios, N., de Leeuw, N.H., Gervais, C., Bonhomme, C., Mauri, F., Chrzanowski, W., Knowles, J.C., Newport, R.J., Wong, A., Gan, Z., and Smith, M.E. (2011) Magnesium incorporation into hydroxyapatite. *Biomaterials*, 32, 1826–1837.
- Lee, H.H., Owens, V.N., Park, S., Kim, J., and Hong, C.O. (2018) Adsorption and precipitation of cadmium affected by chemical form and addition rate of phosphate in soils having different levels of cadmium. *Chemosphere*, 206, 369–375.
- Liu, G., Talley, J.W., Na, C., Larson, S.L., and Wolfe, L.G. (2010) Copper Doping Improves Hydroxyapatite Sorption for Arsenate in Simulated Groundwaters. *Environmental Science & Technology*, 44, 1366–1372.
- Liu, J., Yang, J., Cade-Menun, B.J., Hu, Y., Li, J., Peng, C., and Ma, Y. (2017) Molecular speciation and transformation of soil legacy phosphorus with and without long-term phosphorus fertilization: Insights from bulk and microprobe spectroscopy. *Scientific Reports*, 7, 15354.
- Lowry, N., Han, Y., Meenan, B.J., and Boyd, A.R. (2017) Strontium and zinc co-substituted nanophase hydroxyapatite. *Ceramics International*, 43, 12070–12078.
- Luo, Y., Hughes, J.M., Rakovan, J., and Pan, Y. (2009) Site preference of U and Th in Cl, F, and Sr apatites. *American Mineralogist*, 94, 345–351.
- Matsunaga, K., Murata, H., Mizoguchi, T., and Nakahira, A. (2010) Mechanism of incorporation of zinc into hydroxyapatite. *Acta Biomaterialia*, 6, 2289–2293.
- McLaughlin, M.J., and Singh, B.R. (1999) Cadmium in soils and plants. *Cadmium in soils and plants*, pp. 1–9. Springer.
- Mercier, P.H., Le Page, Y., Whitfield, P.S., Mitchell, L.D., Davidson, I.J., and White, T.J. (2005) Geometrical parameterization of the crystal chemistry of P63/m apatites: Comparison with experimental data and ab initio results. *Acta*

- Crystallographica Section B Structural Science, 61, 635–655.
- Nafel, S., Sham, T., Yiu, Y., and Yates, B. (2001) Calcium L-edge XANES study of some calcium compounds. *Journal of Synchrotron Radiation*, 8, 255–257.
- Neuville, D.R., Cormier, L., Flank, A.M., Briois, V., and Massiot, D. (2004) Al speciation and Ca environment in calcium aluminosilicate glasses and crystals by Al and Ca K-edge X-ray absorption spectroscopy. *Chemical Geology*, 213, 153–163.
- Pan, Y., and Fleet, M.E. (2002) Compositions of the apatite-group minerals: Substitution mechanisms and controlling factors. *Reviews in Mineralogy and Geochemistry*, 48, 13–49.
- Peld, M., Tönsuaadu, K., and Bender, V. (2004) Sorption and desorption of Cd<sup>2+</sup> and Zn<sup>2+</sup> Ions In Apatite-Aqueous Systems. *Environmental Science & Technology*, 38, 5626–5631.
- Petit, S., Gode, T., Thomas, C., Dzwigaj, S., Millot, Y., Brouri, D., Krafft, J.M., Rousse, G., Laberty-Robert, C., and Costentin, G. (2017) Incorporation of vanadium into the framework of hydroxyapatites: importance of the vanadium content and pH conditions during the precipitation step. *Physical Chemistry Chemical Physics*, 19, 9630–9640.
- Politi, Y., Metzler, R.A., Abrecht, M., Gilbert, B., Wilt, F.H., Sagi, I., Addadi, L., Weiner, S., Gilbert, P.U.P.A., and Gilbert, P. (2008) Transformation mechanism of amorphous calcium carbonate into calcite in the sea urchin larval spicule. *Proceedings of the National Academy of Sciences of the United States of America*, 105, 17362–17366.
- Prietzl, J., Dümig, A., Wu, Y., Zhou, J., and Klysubun, W. (2013) Synchrotron-based P K-edge XANES spectroscopy reveals rapid changes of phosphorus speciation in the topsoil of two glacier foreland chronosequences. *Geochimica et Cosmochimica Acta*, 108, 154–171.
- Ravel, B., and Newville, M. (2005) ATHENA, ARTEMIS, HEPHAESTUS: Data analysis for X-ray absorption spectroscopy using IFEFFIT. *Journal of Synchrotron Radiation*, 12, 537–541.
- Sery, A., Manceau, A., and Greaves, N. (1996) Chemical state of Cd in apatite phosphate ores as determined by EXAFS spectroscopy. *American Mineralogist*, 81, 864–873.
- Shannon, R.D. (1976) Revised effective ionic radii and systematic studies of interatomic distances in halides and chalcogenides. *Acta Crystallographica Section A*, 32, 751–767.
- Skwarek, E., and Janusz, W. (2016) Adsorption of Cd (II) ions at the hydroxyapatite/electrolyte solution interface. *Separation Science and Technology*, 51, 11–21.
- Srinivasan, M., Ferraris, C., and White, T. (2006) Cadmium and Lead Ion Capture with Three Dimensionally Ordered Macroporous Hydroxyapatite. *Environmental Science & Technology*, 40, 7054–7059.
- Stammeier, J.A., Purgstaller, B., Hippler, D., Mavromatis, V., and Dietzel, M. (2018) In-situ Raman spectroscopy of amorphous calcium phosphate to crystalline hydroxyapatite transformation. *MethodsX*, 5, 1241–1250.
- Tamm, T., and Peld, M. (2006) Computational study of cation substitutions in apatites. *Journal of Solid State Chemistry*, 179, 1581–1587.
- Terra, J., Dourado, E.R., Eon, J.G., Ellis, D.E., Gonzalez, G., and Rossi, A.M. (2009) The structure of strontium-doped hydroxyapatite: an experimental and theoretical study. *Physical Chemistry Chemical Physics*, 11, 568–577.
- Terra, J., Gonzalez, G.B., Rossi, A.M., Eon, J.G., and Ellis, D.E. (2010) Theoretical and experimental studies of substitution of cadmium into hydroxyapatite. *Physical Chemistry Chemical Physics*, 12, 15490–15500.
- Toby, B.H. (2001) EXPGUI, a graphical user interface for GSAS. *Journal of Applied Crystallography*, 34, 210–213.
- Valsami-Jones, E., Ragnarsdottir, K.V., Putnis, A., Bosbach, D., Kemp, A.J., and Cressey, G. (1998) The dissolution of apatite in the presence of aqueous metal cations at pH 2–7. *Chemical Geology*, 151, 215–233.
- Wang, M., Wu, S., Guo, J., Zhang, X., Yang, Y., Chen, F., and Zhu, R. (2019) Immobilization of cadmium by hydroxyapatite converted from microbial precipitated calcite. *Journal of Hazardous Materials*, 366, 684–693.
- Wilson, R.M., Elliott, J.C., and Dowker, S.E.P. (1999) Rietveld refinement of the crystallographic structure of human dental enamel apatites. *American Mineralogist*, 84, 1406–1414.
- Xu, Y., Schwartz, F.W., and Traina, S.J. (1994) Sorption of Zn<sup>2+</sup> and Cd<sup>2+</sup> on Hydroxyapatite Surfaces. *Environmental Science & Technology*, 28, 1472–1480.
- Yang, T., Wen, W., and Yin, G. (2015) Introduction of the X-ray diffraction beamline of SSRF. *Nuclear Science and Techniques*, 26, 020101.
- Zhang, J.Z., Guo, L., and Fischer, C.J. (2010) Abundance and chemical speciation of phosphorus in sediments of the Mackenzie River Delta, the Chukchi Sea and the Bering Sea: importance of detrital apatite. *Aquatic Geochemistry*, 16, 353–371.
- Zhang, L., Xu, Z., Zhang, X., Yu, H., Zou, Y., Guo, Z., Zhen, X., Cao, J., Meng, X., Li, J., Chen, Z., Wang, Y., and Tai, R. (2015) Latest advances in soft X-ray spectromicroscopy at SSRF. *Nuclear Science and Techniques*, 26, 040101.
- Zhu, Y., Zhu, Z., Zhao, X., Liang, Y., Dai, L., and Huang, Y. (2016) Characterization, dissolution and solubility of cadmium-calcium hydroxyapatite solid solutions at 25 °C. *Chemical Geology*, 423, 34–48.
- Zilm, M.E., Chen, L., Sharma, V., McDannald, A., Jain, M., Ramprasad, R., and Wei, M. (2016) Hydroxyapatite substituted by transition metals: Experiment and theory. *Physical Chemistry Chemical Physics*, 18, 16457–16465.
- Zougrou, I.M., Katsikini, M., Brzhezinskaya, M., Pinakidou, F., Papadopoulou, L., Tsoukala, E., and Paloura, E.C. (2016) Ca L<sub>2,3</sub>-edge XANES and Sr K-edge EXAFS study of hydroxyapatite and fossil bone apatite. *Die Naturwissenschaften*, 103, 60.

MANUSCRIPT RECEIVED APRIL 10, 2020

MANUSCRIPT ACCEPTED MARCH 29, 2021

MANUSCRIPT HANDLED BY JIE XU

### Endnote:

<sup>1</sup>Deposit item AM-22-47560, Online Materials. Deposit items are free to all readers and found on the MSA website, via the specific issue's Table of Contents (go to [http://www.minsocam.org/MSA/AmMin/TOC/2022/Apr2022\\_data/Apr2022\\_data.html](http://www.minsocam.org/MSA/AmMin/TOC/2022/Apr2022_data/Apr2022_data.html)).